International Journal of Heat and Mass Transfer 52 (2009) 250–259

Contents lists available at ScienceDirect

International Journal of Heat and Mass Transfer

journal homepage: www.elsevier.com/locate/ijhmt

Magnetohydrodynamic natural convection in a vertical cylindrical cavity with sinusoidal upper wall temperature

S.C. Kakarantzas [a,1], I.E. Sarris [a,b,1], A.P. Grecos [a,1], N.S. Vlachos [a,*,1]

[a] Department of Mechanical and Industrial Engineering, University of Thessaly, Athens Avenue, 38334 Volos, Greece
[b] Physique Statistique et Plasmas, CP 231, Université Libre de Bruxelles, 1050 Brussels, Belgium

ARTICLE INFO

Article history:
Received 9 November 2007
Available online 29 August 2008

Keywords:
Natural convection
Magnetohydrodynamics
Liquid metals
Sinusoidal wall temperature
Computational fluid dynamics

ABSTRACT

A series of numerical simulations were performed in order to study liquid metal MHD natural convection in a vertical cylindrical container with a sinusoidal temperature distribution at the upper wall and the other surfaces being adiabatic. Starting from the basic hydrodynamic case, the effect of vertical (axial) and horizontal magnetic fields is assessed. Depending on the magnitude of the Rayleigh and Hartmann numbers, both turbulent and laminar (azimuthally symmetric or not) flows are observed. The results show that the increase of Rayleigh number promotes heat transfer by convection while the increase of Hartmann number favors heat conduction. The vertical magnetic field reduces the Nusselt number more than the horizontal. The circulation patterns for the most convective cases are confined close to the top corner of the container with the simultaneous formation of a secondary flow pattern at the bottom corner, while for the more conductive cases only one circulation pattern exists covering the entire domain.
© 2008 Elsevier Ltd. All rights reserved.

1. Introduction

Magnetohydrodynamic natural convection in cylindrical containers are of great importance considering the number of technological and industrial applications involved. Such configurations include the production of steel, aluminum, high performance super-alloys or crystals [1]. In the case of crystal growth, for example, magnetic fields are used to suppress the convective motion induced by the arising strong fluxes in order to control the flow in the melt and consequently the crystal quality [2]. Except of the industrial processing applications where the flow in cylindrical containers are important, another case with strong theoretical interest is the flow of liquid metals in fusion blankets [3].

A number of experimental and theoretical studies have been performed for these flows. Oreper and Szekely [4] and Kim et al. [5] numerically simulated the flow in a vertical Bridgman–Stockbarger configuration and demonstrated the influence of the applied magnetic field on the intensity of convection in the melt. Chandrasekhar [6] studied the influence of a vertical magnetic field on convection arising in a fluid layer heated from below, while Karcher et al. [7] investigated the effect of a vertical magnetic field on the convective heat transfer in a liquid metal heated locally from above. Baumgartl and Mueller [8] compared three MHD models of different complexity in order to calculate the effect of magnetic damping of the fluid flow in a cylindrical cavity heated from below. Fedoseyev et al. [9] performed a numerical investigation for thermal convection flow in a semiconductor melt with strong static magnetic field and compared three different numerical models.

Periodic wall heat fluxes are of great interest in engineering applications such as the design of cooling tubes for nuclear reactors or heat exchangers of Stirling engines [10]. The sinusoidal wall heat flux is one of the simplest types of periodic heating and is encountered in many studies. Sarris et al. [11] investigated numerically the flow and heat transfer in a two-dimensional square cavity with a sinusoidal temperature profile at the upper wall and adiabatic conditions on the bottom and sidewalls. Pearlstein and Dempsey [12] studied a laminar tube flow subjected to axially varying wall heat flux in the form of a sinusoidal or hyperbolic tangent distribution. Barletta and Zanchini [13] studied the stationary and laminar forced convection in a circular tube with a sinusoidal axial distribution of wall heat flux, evaluating the heat transfer via the temperature fields and local Nusselt numbers. Dalal and Das [14] studied a steady laminar natural convection in a two-dimensional enclosure with one wavy and three flat walls with a sinusoidal top wall temperature profile. Velocity and temperature fields were calculated while the heat transfer was assessed via the Nusselt number. The effect of Rayleigh number, amplitude and number of undulations on the flow pattern and heat transfer was studied. The heat transfer mode remains conductive up to $Ra = 10^3$ and, for greater Ra values, convection starts to dominate as it is con-

* Corresponding author. Tel.: +30 24210 74094; fax: +30 24210 74085.
E-mail address: vlachos@mie.uth.gr (N.S. Vlachos).
[1] E-mail: fluids@mie.uth.gr

0017-9310/$ - see front matter © 2008 Elsevier Ltd. All rights reserved.
doi:10.1016/j.ijheatmasstransfer.2008.06.035

Nomenclature

B_0	magnitude of the external magnetic field (kg/(s^2 A))
$C=\sqrt{r_o^2+z_o^2}$	distance of the circulation center from the origin (m)
g	gravity acceleration (m/s^2)
H	height of the cylinder (m)
$Ha=\sqrt{\sigma/\rho\nu}B_0R$	Hartmann number
Nu	Nusselt number
p	fluid pressure (N/m^2)
$Pr=\nu/\alpha$	Prandtl number
r,θ,z	spatial coordinates
R	radius of the cylinder (m)
$Ra=g\beta\Delta TR^3/\nu\alpha$	Rayleigh number
t	time (s)
$\mathbf{u}$	non-dimensional velocity vector
u_z,u_r,u_θ	non-dimensional axial, radial, circumferential velocity components

Greek letters

α	thermal diffusivity (m^2/s)
β	coefficient of thermal expansion (1/K)
ν	fluid kinematic viscosity (m^2/s)
ρ	fluid density (kg/m^3)
σ	electric conductivity (ms^3 A^2/kg)
Φ	electric potential (m^2 kg/s^3 A)
Ψ	non-dimensional stream function

Subscripts

c	cold
o	position of circulation center
w	indicating a wall

cluded from the average Nusselt number which remains constant for Ra up to 10^3 and then starts changing. Because of the nature of the imposed boundary conditions, there are two large vortices formed. Bilgen and Ben Yedder [15] carried out a numerical study of natural convection in rectangular enclosures, with one vertical wall heated and cooled sinusoidally and all the others insulated. Two cases were considered: (a) the lower part of the wall is heated while the upper part is cooled and (b) the upper part is heated and the lower part is cooled. The heat transfer was studied in order to determine the thermal penetration in the enclosure. It was found that the penetration approaches 100% at high Rayleigh numbers in the first case, while in the second it approaches about 70%.

The present work was motivated by the numerical and experimental work of Karcher et al. [7] where the electron beam evaporation of liquid metals was studied. In this industrial application, a localized temperature distribution at the surface of the liquid metal is applied and the external magnetic field is used for control and stabilization of the fluid motion and heat transfer. Similarly to Karcher et al. [7], the flow of a liquid metal (small Prandtl number, $Pr = 0.0321$) placed in a vertical cylindrical container is presently considered. The upper surface has a sinusoidal temperature profile and the other surfaces are considered adiabatic. The effect of the magnetic field is assessed for the cases of uniform vertical and horizontal magnetic fields. The primary objectives of the present study are, firstly to establish the basic hydrodynamic flow and secondly to study the effect of the magnetic field on the flow and heat transfer. Numerical results were obtained for Rayleigh numbers in the range 10^2–10^6 and for Hartmann numbers from 0 to 50. Both unsteady and laminar flows are observed depending on the combination of Rayleigh and Hartmann numbers. The results are presented in the form of streamlines, isotherms and Nusselt number distributions.

2. Problem description and model setup

A cylindrical container, shown schematically in Fig. 1, is considered with a radius R and height $H(H/R = 1)$. A sinusoidal temperature distribution $T_w(r) = T_c + \frac{\Delta T}{2}(1 + \cos(\pi r/R))$ is applied on the upper wall while the lower and cylindrical surfaces are assumed to be adiabatic. T_c is the temperature at the corner formed by the upper wall with the cylindrical wall, ΔT is the difference between the maximum and minimum temperatures at the upper wall. For the magnetohydrodynamic case a vertical (axial) or horizontal uniform magnetic field of magnitude B_0 is applied. The low magnetic Reynolds number model for the magnetohydrodynamic flow cases and the Boussinesq approximation for buoyancy are also adopted [16,17].

The magnetohydrodynamic equations were made dimensionless using as characteristic quantities the radius R of the cylinder, the reference velocity $u_0 = \alpha/R$, the temperature difference ΔT and the magnitude of the external magnetic field B_0. Consequently, we have $(r^*, z^*) = (r, z)/R$ for the radial and axial coordinates, $p^* = pR^2/\rho\alpha^2$ for the dimensionless pressure, $\mathbf{u}^* = \mathbf{u}/u_0$ for the velocity vector with components u_z, u_r and u_θ for the axial, radial and azimuthal components, respectively. We also have $T^* = (T - T_c)/\Delta T$ for the temperature, $t^* = t\alpha/R^2$ for the time, $\Phi^* = \Phi/\alpha B_0$ for the electric potential and $\mathbf{J}^* = \mathbf{J}R/\sigma\alpha B_0$ for the current density; where the quantities without the asterisks are the dimensional ones, ρ is the fluid density, α is the thermal diffusivity and σ the electrical conductivity. Thus, the governing equations may be written in dimensionless form (omitting the asterisks):

$$\nabla\cdot\mathbf{v}=0, \tag{1}$$

$$\frac{\partial\mathbf{u}}{\partial t}+\mathbf{u}\cdot\nabla\mathbf{u}=-\nabla p+RaPrT\mathbf{e_z}+Pr\nabla^2\mathbf{u}+PrHa^2(\mathbf{J}\times\mathbf{e_B}), \tag{2}$$

$$\frac{\partial T}{\partial t}+\mathbf{u}\cdot\nabla T=\nabla^2T, \tag{3}$$

$$\mathbf{J}=-\nabla\Phi+\mathbf{u}\times\mathbf{e_B}, \tag{4}$$

$$\nabla^2\Phi=\nabla\cdot(\mathbf{u}\times\mathbf{e_B}), \tag{5}$$

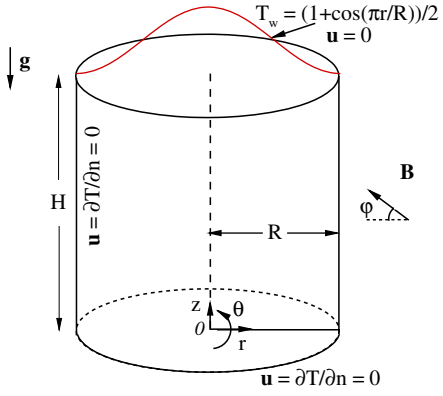

Fig. 1. Flow geometry and boundary conditions.

where $\mathbf{e_z}$ is the unit vector in the axial direction, $\mathbf{e_B}$ is the unit vector in the direction of the external magnetic field, and the gradient operator in cylindrical coordinates is given by $\nabla = \frac{\partial}{\partial r} + \frac{1}{r}\frac{\partial}{\partial \theta} + \frac{\partial}{\partial z}$.

The flow depends on three dimensionless parameters: the Rayleigh number (Ra), the Prandtl number (Pr) and the Hartmann number (Ha) which are defined as:

$$Ra = \frac{g\beta\Delta T R^3}{\nu\alpha}, \quad Pr = \frac{\nu}{\alpha}, \quad \text{and} \quad Ha = B_0 R\sqrt{\frac{\sigma}{\rho\nu}}, \tag{6}$$

where g is the gravity acceleration, β the volumetric thermal expansion coefficient and ν the kinematic viscosity of the fluid.

As for the boundary conditions, the liquid metal obeys the no-slip condition at the walls, $u_z = u_r = u_\theta = 0$ for $z = 0$ and 1 or $r = 1$, and the symmetry condition along the cylinder axis. The bottom and cylindrical walls are considered adiabatic, $\partial T/\partial n = 0$ for $z = 0$ or $r = 1$, and the upper wall has a temperature distribution, $T = \frac{1}{2}(1 + \cos(\pi r))$ for $z = 1$.

In order to study the heat transfer characteristics of the fluid, the local Nusselt number at the upper wall is calculated via the expression:

$$Nu(r,\theta) = [-\partial T/\partial z]_{z=1}. \tag{7}$$

Then, an averaged local Nusselt number on the azimuthal direction can be defined as $Nu(r) = \frac{1}{2\pi}\int_0^{2\pi} Nu(r,\theta)\,d\theta$. It must also be noted that a stream function Ψ is calculated from the velocity fields averaged in the azimuthal direction via the definition: $u_r = \partial\Psi/\partial z$, assuming that $\Psi = 0$ at $r = 1$ and $z = 0$.

3. Numerical details

Numerical simulations were performed for various Rayleigh and Hartmann numbers. While most of the studied cases result in laminar flow, the higher Rayleigh number cases (with or without magnetic field) result in turbulent flow. The direct numerical method and the fine grid used in the study are able to capture most of the turbulent dynamics. The governing Eqs. (1)–(5) were discretized in a staggered non-uniform mesh with second-order accurate finite difference schemes following the same procedure as in [18]. The resulting system of algebraic equations was solved with a fractional step approach [19] where a semi-implicit scheme was used for the time integration. Initially, a non-solenoidal velocity field is evaluated and is used in the calculation of an intermediate pressure field. In the second step, by using both intermediate fields, the solenoidal velocity field and the pressure field are obtained. The diffusion terms were advanced in time with a Crank–Nicolson method, while the non-linear, the buoyancy and Lorentz force terms with an economic third-order Runge–Kutta method [18,20,21]. The Poisson equations for the pseudo-pressure and the electric potential (located at the center of each computational cell) were solved using a transform method with modified wavenumbers corresponding to the second-order central difference scheme, together with tridiagonal matrix inversion using the FISHPACK library [22].

The present numerical method was tested successfully against the numerical results of Sarris et al. [11] and Karcher et al. [7]. There are some differences between these two studies and the present flow. In Sarris et al. [11] the study is limited only to the hydrodynamic flow and it refers to an orthogonal cavity in which the upper surface is at sinusoidal temperature and the other surfaces are considered adiabatic. This work was used to verify the thermal boundary conditions. In Karcher et al. [7], a cylindrical geometry is considered in which the upper surface is heated locally close to the axis, with the rest of the surface being isothermal, and also an external homogeneous magnetic field is applied in the axial direction. Fig. 2a presents a comparison of the present results with those of reference [11] and show that the most sensitive quantity to the grid arrangement (i.e. local Nusselt number at the upper surface) is very closely predicted also by the present model. In Fig. 2b, a comparison is presented between the results of this model and those of reference [7] in terms of the maximum value of the temperature versus the Hartmann number, with very good agreement.

For a properly resolved direct numerical simulation, especially in the case of turbulent or MHD flow, the features of the specific flow, heat transfer and boundary layers must be considered. In particular, the increase of Ha results to thinner Hartmann layers at the walls normal to the magnetic field of thickness $\sim 1/Ha$, while the increase of Ra results to thinner boundary layers and smaller Kolmogorov and Batchelor scales. All these requirements were taken into account in the present numerical simulations by using the analysis proposed by Grötzbach [23] where the appropriate Kolmogorov scale, η, can be a function of Nu for fluids with $Pr < 1$. The value of the grid sizing depends on Nu which is given for MHD natural convection flows according to Aurnou and Olson [24] by $Nu \propto (Ra/Ha^2)^{\frac{1}{2}}$. As a result, non-uniform grids were used for the simulation of the cases $Ra = 10^2$ to 10^6. More specifically, a grid of $49 \times 49 \times 49$ cells was used in the cases $Ra = 10^2$ to 10^4, $65 \times 65 \times 65$ cells for $Ra = 10^5$ and $97 \times 97 \times 97$ cells for $Ra = 10^6$ in the azimuthal, radial and axial directions, respectively. It must be noted that for $Ra \leqslant 10^5$, the resulting flow is laminar and axisymmetric in the hydrodynamic case. Also when the imposed magnetic field is aligned with the axial direction, the flow is axisymmetric but not in the case of horizontal magnetic field or turbulent flow. Finally, it should be noted that, unless it is stated differently, all the quantities for the turbulent cases shown here correspond to azimuthally averaged fields. In the case of turbulent flows the quantities are time averaged when the flow is stationary.

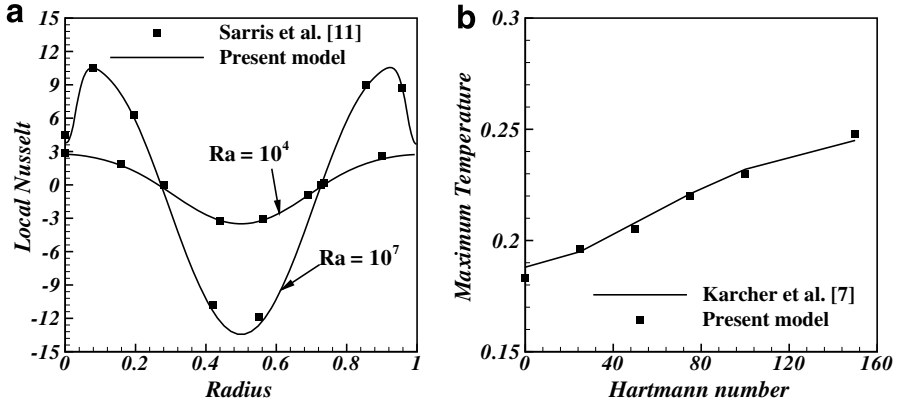

Fig. 2. Comparison of the present model with the results of Sarris et al. [11] (left), and the results of Karcher et al. [7] (right).

Table 1
Grid independence test for the case of axial magnetic field ($Ra = 10^5, Ha = 25$)

Grid:	$65 \times 65 \times 65$	$81 \times 81 \times 81$	$97 \times 97 \times 97$	$121 \times 141 \times 141$
$u_{r,max}$	10.201	10.184	10.193	10.146
$u_{z,max}$	5.757	5.764	5.766	5.743

The above requirements for the construction of the grid are tested by performing also a grid independence test. For this purpose, the case of $Ra = 10^5$ and $Ha = 25$ was chosen and an axial magnetic field was applied. The range of the grids used in these tests and the results of each case are presented in Table 1. The comparison of the maximum values of the radial and axial velocity components indicates that the changes are smaller than 0.5% and thus the grid selection is appropriate.

4. Results and discussion

4.1. Basic hydrodynamic flow

In Figs. 3–7, the effect of the Rayleigh number is demonstrated in terms of the stream function, velocity and temperature fields, and the local Nusselt number distribution. For $Ra = 10^4$ and 10^5, the flow is laminar and axisymmetric. When the Rayleigh number increases to 10^6, the flow becomes turbulent resulting to higher velocity and temperature gradients. In comparison to the simulations of Sarris et al. [11], the present flow can become turbulent at a lower Rayleigh number because of the low Prandtl number of the fluid used.

In Fig. 3, the stream function (left column) and isotherm distributions (right column) are shown for the hydrodynamic cases with $Ra = 10^4, 10^5$ and 10^6 (top to bottom), respectively. For $Ra = 10^6$ the flow is turbulent, and the presented distributions correspond to azimuthally and time averaged fields. It is observed that the increase of the Rayleigh number enhances the motion of the fluid as indicated by the higher values of the stream function. The fluid is ascending near the axis of the cylindrical cavity, due to the higher temperature of the top surface, it then travels towards the edges and it descends along the vertical (cylindrical) wall. In the case of $Ra = 10^4$ the flow is characterized by one circulation zone filling all the domain, while for $Ra = 10^5$ a secondary circulation appears near the corner of the vertical wall with the bottom of the cavity. The intensity of the secondary circulation is significantly lower but it increases with the increase of the Rayleigh number. As a con-

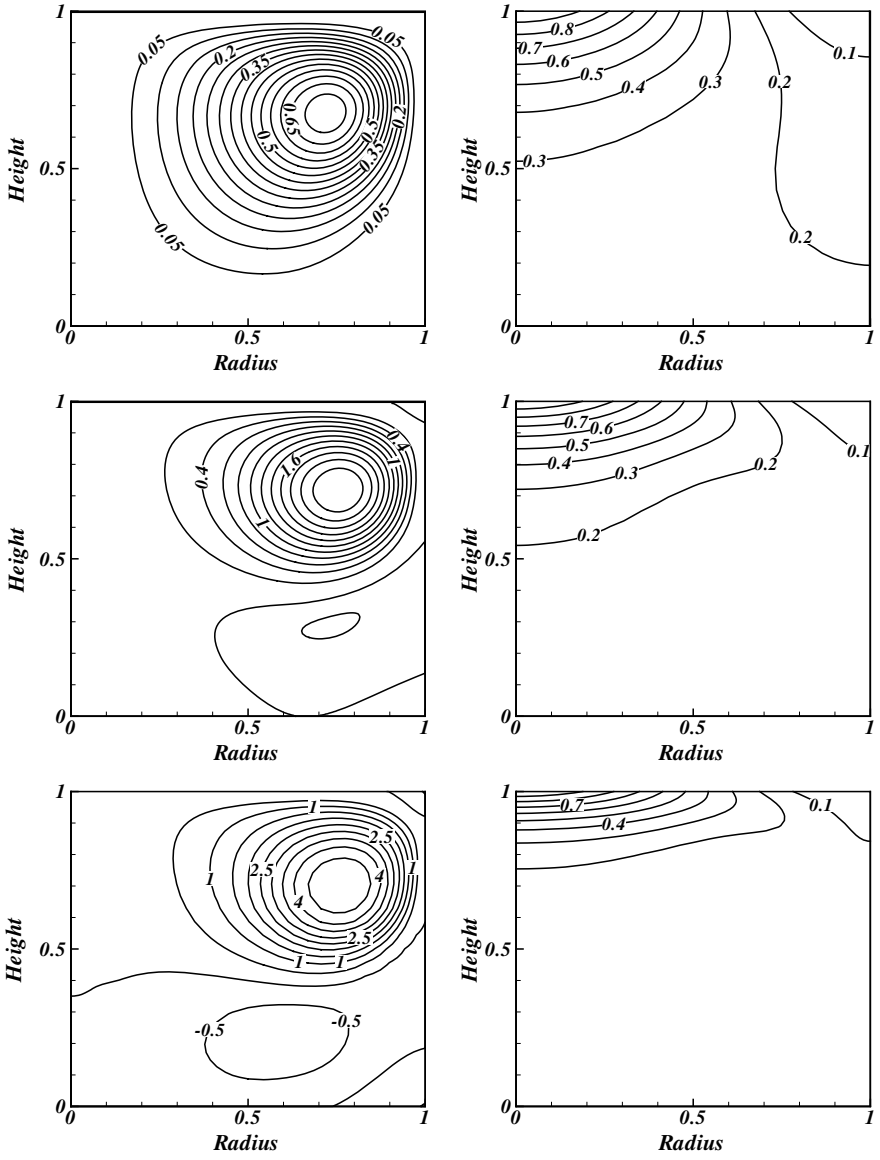

Fig. 3. Azimuthally averaged stream function (left) and temperature distribution (right) for $Ra = 10^4$ (upper), $Ra = 10^5$ (middle) and $Ra = 10^6$ (lower).

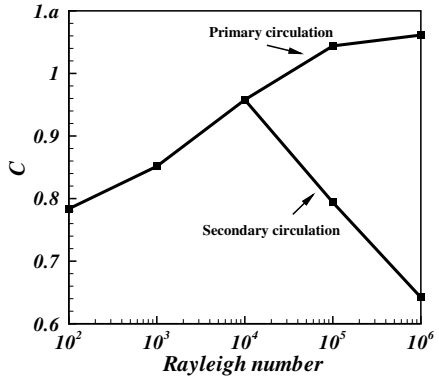

Fig. 4. Variation of the position of circulation center with *Ra* for the hydrodynamic cases.

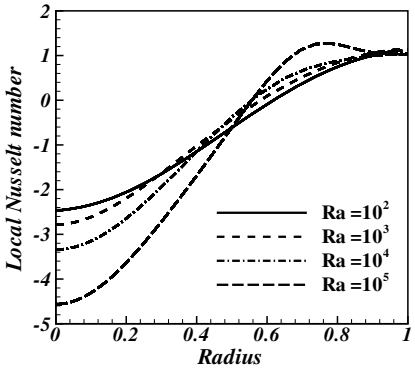

Fig. 6. Comparison of the local Nu number distribution for $Ha = 0$ and $Ra = 10^2$ to 10^5.

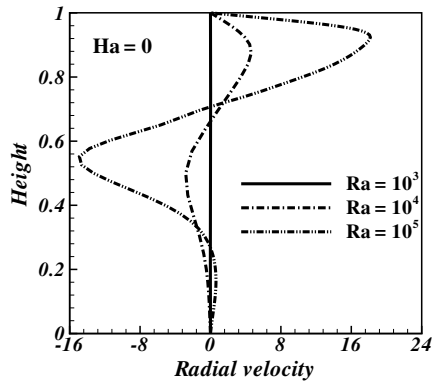

Fig. 5. Comparison of the axial distribution on the radial velocity at $r = 0.8$ for $Ra = 10^3$ to 10^5 and $Ha = 0$.

sequence, there are two extremes of the stream function for $Ra = 10^5$ and 10^6, indicating two opposite rotating circulation patterns. This is confirmed in Fig. 4 where the distance C of the centers of the circulations from the origin $(z = 0, r = 0)$ are presented versus the Rayleigh number. It should be noted that C is defined as $C = \sqrt{r_o^2 + z_o^2}$, where r_o and z_o are the coordinates of the center of the circulation. The increase of the Rayleigh number results (as in Sarris et al. [11]) in an increase of the local convection heat transfer (heating or cooling) from the top surface. As a consequence hot fluid is confined very close to the upper wall and the penetration of heat in the bulk fluid is more difficult. The thinner thermal boundary layers and their interaction with the adiabatic cylindrical sidewall are responsible for the flow separation and the formation of the secondary circulation.

In Fig. 5, a comparison is shown of the axial distribution of the radial velocity at $r = 0.8$ for $Ra = 10^3, 10^4$ and 10^5. For $Ra = 10^3$, the radial velocity is very small. As the Rayleigh number takes higher values, the motion of the fluid is enhanced and consequently the velocities are becoming higher while their distribution remains almost similar in shape. It is interesting to observe that the velocities in the lower part of the geometry, and more specifically at dimensionless height $z \leqslant 0.25$, are taking values very close to zero. In the upper part of the domain, two regions are formed where the velocity changes sign from positive to negative. Particularly the sign is negative for $0.25 < z < 0.7$ and positive for $0.7 < z < 1$. Close to the points $z = 0.25$, 0.7 and 1.0, the velocities are almost equal to zero.

The increase of *Ra* has a significant effect on the local *Nu* distribution at the upper wall as shown in Fig. 6. Because of the higher temperature gradients developing as the temperature difference is becoming larger, the absolute values (heating or cooling) of the local *Nu* increase, while the shape of the distribution remains almost the same. Thus, the increase of the Rayleigh number favors the convection heat transfer mechanism against conduction. It should be noted that, because of the use of adiabatic conditions at the sidewall and the bottom of the container, the average *Nu* is zero in all cases, for steady state condition.

For $Ra = 10^6$, the flow becomes turbulent as indicated by the spectral distribution of the averaged kinetic energy versus the azimuthal wave numbers in Fig. 7a. For the calculation of the energy, only contributions of the bulk flow, away from the walls, were con-

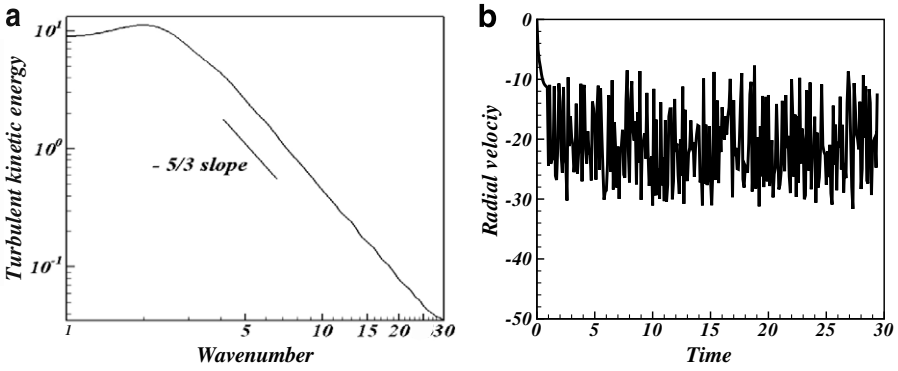

Fig. 7. Spectral distribution of the averaged kinetic energy versus the azimuthal wave numbers (left), and time variation of radial velocity (right) at point (θ: 180°, r: 0.5, z: 0.5) for $Ra = 10^6$.

sidered. Moreover, the temporal variation of the radial velocity at the position (θ: 180°, r: 0.5, z: 0.5) is changing rapidly as shown in Fig. 7b.

4.2. Vertical (axial) magnetic field

When a vertical (axial) magnetic field is imposed, some interesting changes are observed in the motion of the fluid and the resulting heat transfer. In the case of turbulent flow, the presence of the magnetic field results in the stabilization of the flow turning it to laminar and axisymmetric. In general, the magnetic field suppresses the fluid motion and reduces the rate of heat transfer. In Figs. 8 and 9, streamlines and isotherms are presented for $Ha = 10, 25$ and 50, and for $Ra = 10^4$ and 10^5, respectively. It is observed that the increase of the magnetic field strength results to the damping of the fluid motion as it is indicated by the reduced values of the stream function. This behavior of the Lorentz force is known, Davidson [3], and can also explain the distribution of the isotherms. As the Hartmann number increases, the temperature gradients become less abrupt and the convection effects become less intense resulting to smaller velocities. Thus, the increase of the magnetic field favors the conduction heat transfer, which dominates at higher Ha values. As a result of the more extended and slower circulating flow, the location of the center of the circulation is moving to the position where convection sets on (i.e. forms one toroidal vortex aligned in the θ direction with its center in the mid cross-section of the container). For $Ra = 10^4$, the above phenomenon is vigorous until the Hartmann number reaches the value 25 and for greater values thereon it is weaken, showing no significant change in the flow pattern. This means that the center of the circulation remains almost at the same position and conduction is the dominant heat transfer mechanism. This is confirmed in Fig. 10a where the distance of the center of the circulation from the origin is presented versus the Hartmann number. In Fig. 10b, the same distance is presented for the case of $Ra = 10^5$. In both cases, the center of the circulation with the increase of the Hartmann number follows the same trend. Another prominent result of the influence of the magnetic field is the disappearing of the secondary circulation with increasing magnetic field. As Fig. 10b shows for the case of $Ra = 10^5$, two circulation regions appear in the flow for $Ha < 20$ but only one survives at $Ha > 20$.

For the case of $Ra = 10^6$ and $Ha = 0$, the flow is turbulent and as Ha increases the flow is stabilized and becomes laminar. In Fig. 11a and b the time variation of the axial and the radial velocity compo-

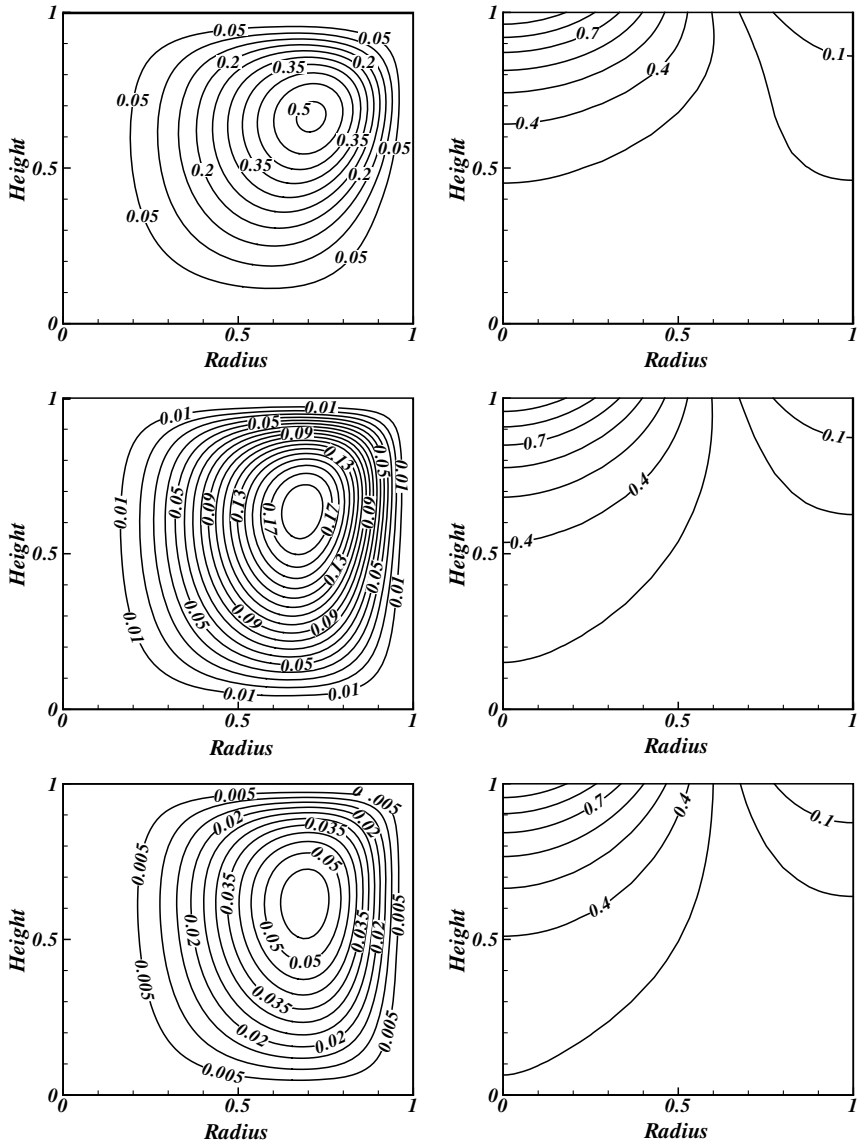

Fig. 8. Streamlines (left) and isotherms (right) for $Ra = 10^4$ and $Ha = 10$ (upper), 25 (middle) and 50 (lower).

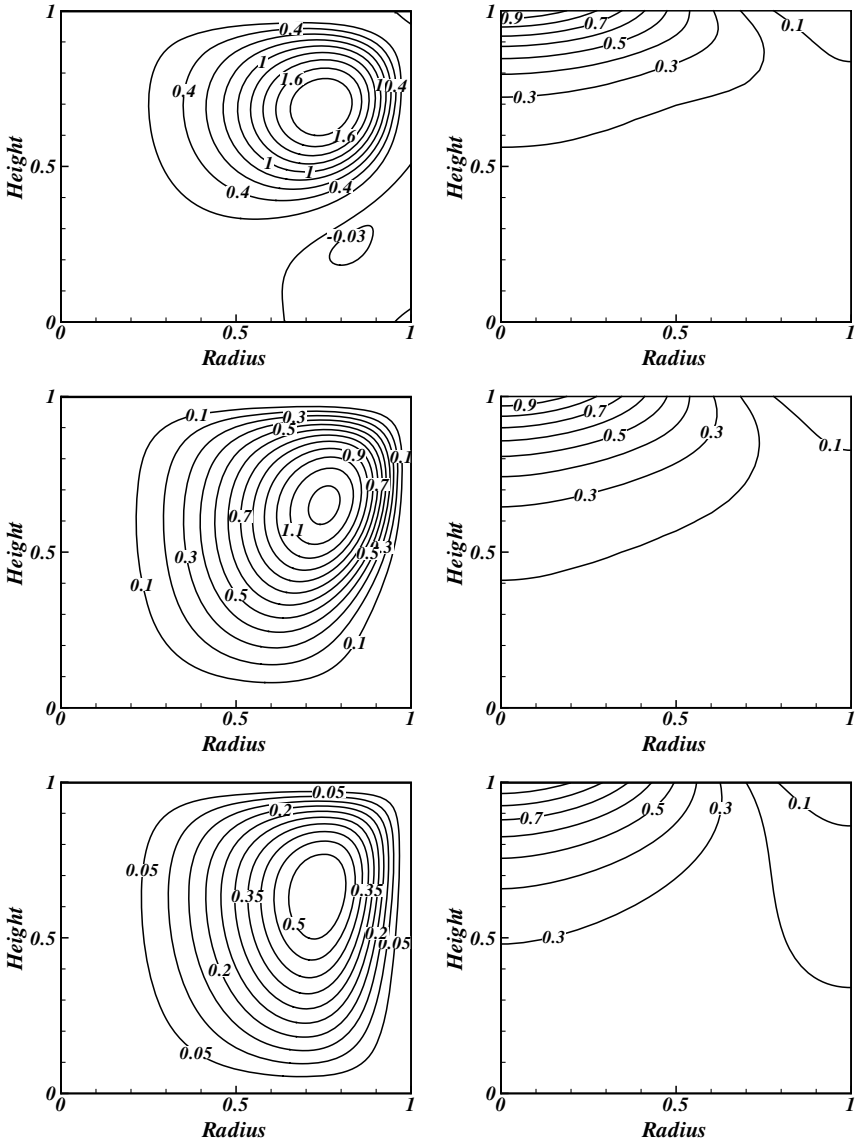

Fig. 9. Streamlines (left) and isotherms (right) for $Ra = 10^5$ and for $Ha = 10$ (upper), 25 (middle) and 50 (lower).

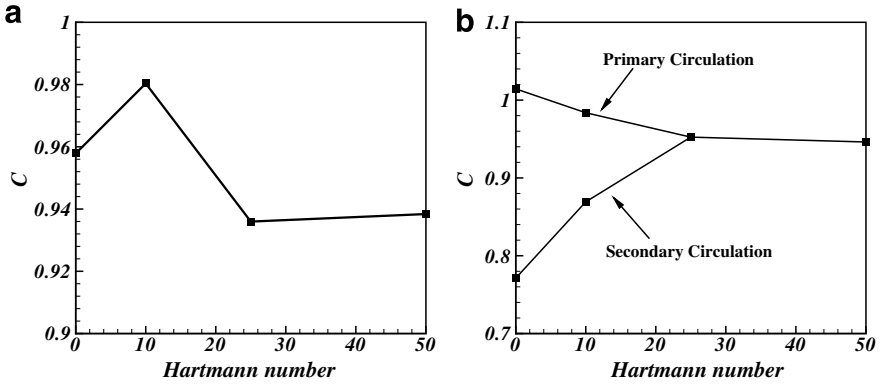

Fig. 10. Variation of the position of circulation center with *Ha* for $Ra = 10^4$ (left) and for $Ra = 10^5$ (right).

nents, respectively, are presented at the position (θ: 180°, r: 0.5, z: 0.5) for Ha = 0, 10, 25 and 50. It is clearly shown that the increase of *Ha* results in the minimization and, for higher *Ha* values, to the vanishing of the velocity fluctuations. It must be noted that when the flow is becoming laminar due to the applied magnetic field parallel to gravity, it retains its axisymmetry. For the monitoring point of Fig. 11, the increase of *Ha* results progressively in higher mean velocities for the turbulent cases. However, for higher *Ha* values,

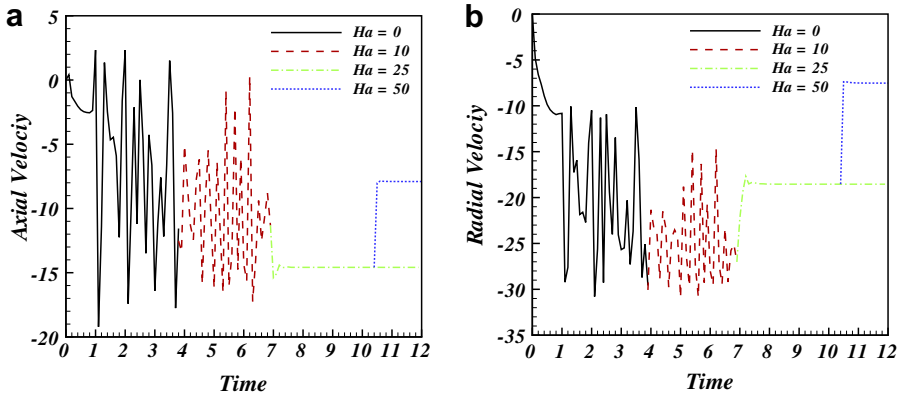

Fig. 11. Time variation of axial (left) and radial (right) velocity at point (θ: 180°, r: 0.5, z: 0.5) for $Ra = 10^6$ and various Ha.

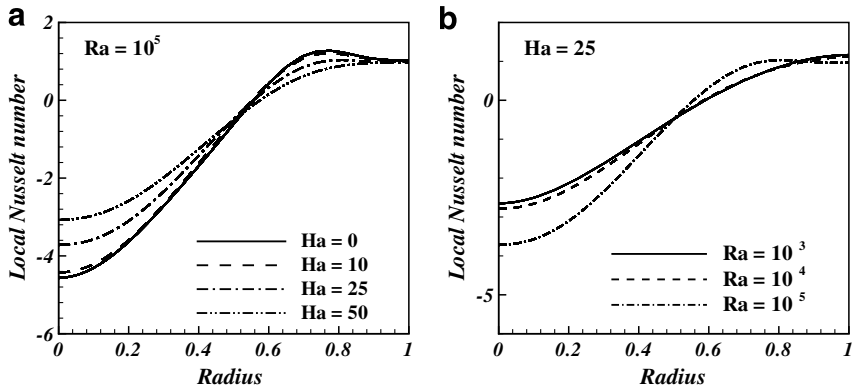

Fig. 12. Comparison of local Nu number distribution: (left) $Ra = 10^5, Ha = 0, 10, 25$ and 50, (right) $Ha = 25$, $Ra = 10^3, 10^4$ and 10^5.

the flow is laminarized and the damping effect of the magnetic field reduces the fluid velocities.

Regarding the heat transfer mechanism, Figs. 8 and 9 show that the increase of the magnetic field results in smoother temperature gradients and thus, the local Nusselt number should be reduced. In Fig. 12a the local Nusselt number distribution is presented for $Ha = 10, 25$ and 50 at $Ra = 10^5$ confirming the above observation. In Fig. 12b the same distribution is depicted for $Ra = 10^3, 10^4$ and 10^5 at $Ha = 25$, showing the increase of the Nusselt number as the Rayleigh number increases.

4.3. Horizontal magnetic field

When a horizontal magnetic field is applied, an interesting difference takes place in contrast to the hydrodynamic and the vertical magnetic field cases. As shown above, in the laminar hydrodynamic cases the flow retains an azimuthal symmetry which is also true in the cases where an axial magnetic field is applied. When the magnetic field is applied in the horizontal direction the above axisymmetry is not present anymore. More specifically, jets of the descending fluid are developing near the walls parallel to the magnetic field, while near the walls normal to it the fluid decelerates. Fig. 13 shows the regions near the maximum and minimum values of the axial velocity isosurfaces, for the cases $Ra = 10^4$ (upper) and $Ra = 10^5$ (lower) for $Ha = 0$ (left) and $Ha = 50$ (right) and confirms the above observation. For the hydrodynamic case, the isosurfaces form ascending and descending axisymmetric rings. Because of the pair of jets formed near the walls parallel to the horizontal magnetic field, the fluid also ascends near the axis of the container forming a pair of jets.

The loss of the axisymmetry is a combined result of the magnetic field because of the formation of the Hartmann and side layers near the walls normal and parallel to the magnetic field, respectively. Their thickness is a function of the Hartmann number, i.e. $\sim 1/Ha$ and $\sim 1/Ha^2$ for the Hartmann and the side layer, respectively. More specifically in the Hartmann layers the motion of the fluid reduces in larger degree than in the side layers. As a consequence the azimuthal symmetry of the flow is lost. A thin Hartmann layer is formed near the $\theta = 0°$ region, while a thicker

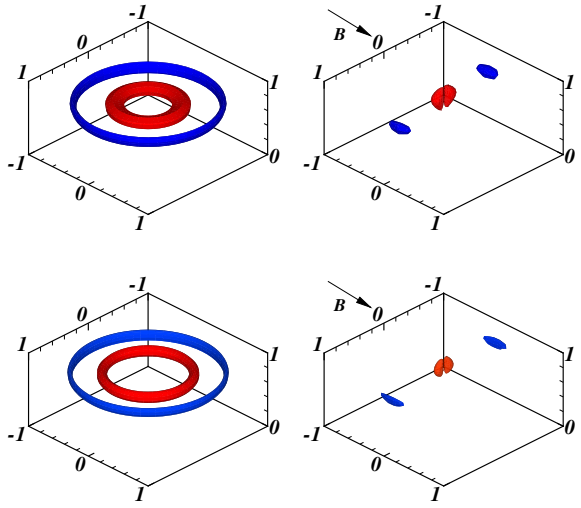

Fig. 13. Axial velocity distribution for $Ha = 0$ (left) and 50 (right) at $Ra = 10^4$ (upper) and $Ra = 10^5$ (lower).

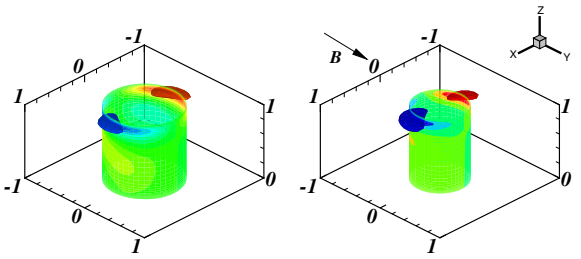

Fig. 14. Azimuthal Lorentz force distribution for $Ha = 25$ (left) and 50 (right) at $Ra = 10^4$.

side layer is formed in the $\theta = 90^\circ$ area. As a result, the fluid velocity is higher near the side layers and lower near the Hartmann layers. The impact of these layers in the flow is expressed via the Lorentz force, which has the tendency to resist the fluid motion. The Lorentz force is always retarding the fluid and it is stronger where the velocity is higher. As shown in Fig. 14, the distribution of the azimuthal component of the Lorentz force for $Ha = 25$ (left) and $Ha = 50$ (right) is higher near the $\theta = 90^\circ$ region where the velocity is higher.

As it is already mentioned, for the case $Ra = 10^6$ and $Ha = 0$ the flow is fully turbulent. When a magnetic field is applied, the turbulent flow becomes steady state and laminar. This is happening progressively with increasing Ha number, as shown in Fig. 15, where the time variation of the axial velocity component for $Ha = 0$ to 50 is depicted at position (θ: 180°, r: 0.5, z: 0.5). The simulations for higher Ha were restarted from the lower Ha cases. It is observed that while for $Ha = 0$ the velocity fluctuates in time, for the case $Ha = 50$ there is no change in time. The velocity fluctuations, as in the case of the axial magnetic field of Fig. 11, are reduced with increasing Ha.

As it concerns the heat transfer, the magnetic field suppresses the fluid motion and as a result the Nusselt number decreases with increasing Hartmann number. This is shown in Fig. 16a where the Nusselt number distributions for the cases $Ha = 10, 25$ and 50 with $Ra = 10^5$ at $\theta = 0^\circ$ are compared. It must be noted that when the magnetic field is applied in the horizontal direction, the Nusselt number is slightly changing azimuthally as a result of the non-axisymmetric flow and temperature fields. In Fig. 16b the Nusselt number distribution is presented at the angles $\theta = 0^\circ$ and $\theta = 90^\circ$ for $Ra = 10^6$ and $Ha = 50$ confirming the above observations.

Another interesting observation is that, when the magnetic field is imposed in the axial direction, the value of the Nusselt number, and as a consequence the heat transfer mechanism, is affected more than for the case of the horizontal magnetic field at the same Hartmann number. Thus, the Nusselt number is higher in the case of the horizontal magnetic field. This is shown in Fig. 17 where the difference of the Nusselt number corresponding to the two magnetic field directions is presented for the same Rayleigh and Hartmann numbers ($Ra = 10^6, Ha = 50$). It is clearly shown that the Nusselt number difference is considerable in all the upper surface, except the region $r = 1$. The reason is that the axial magnetic field forms Hartmann layers at the upper and bottom surfaces (rather than at the cylindrical wall as in the case of the horizontal magnetic field) and the flow is uniformly damped with less heat convected.

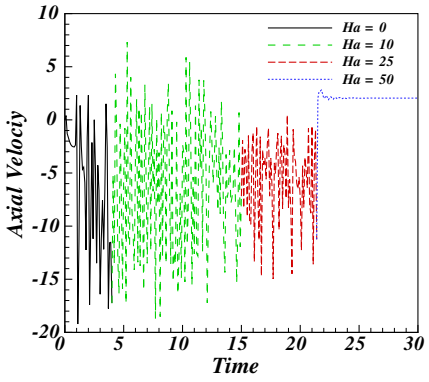

Fig. 15. Temporal variation of axial velocity at point (θ: 180°, r: 0.5, z: 0.5) for $Ra = 10^6$ and $Ha = 0, 20, 25$ and 50.

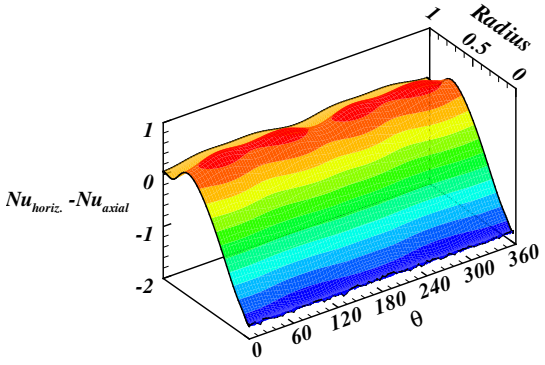

Fig. 17. Distribution of local Nusselt number difference for vertical and horizontal magnetic fields ($Ra = 10^5, Ha = 50$).

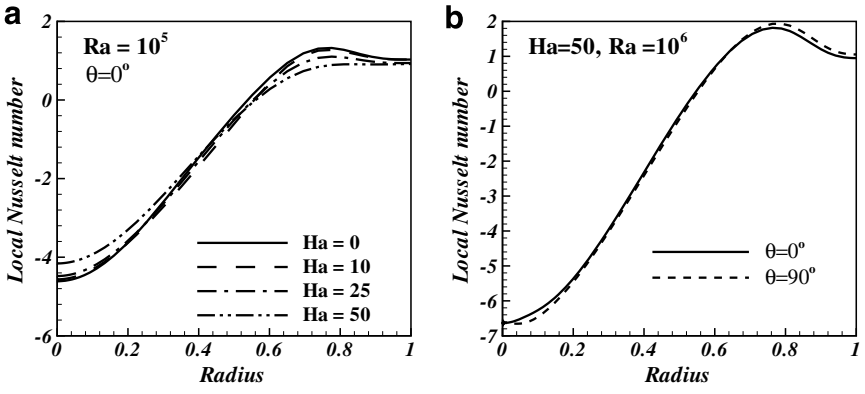

Fig. 16. Radial distribution of local Nusselt number: (left) $\theta = 0^\circ, Ra = 10^5, Ha = 10, 25$ and 50, (right) $Ra = 10^6, Ha = 50, \theta = 0^\circ$ and 90°.

5. Conclusions

For the hydrodynamic case, the present results show that the increase of the Rayleigh number promotes convection. For higher *Ra* values, the flow is becoming turbulent and the heat transfer is enhanced. More specifically, for the range of $Ra = 10^2$ to 10^5, the flow is laminar and axisymmetric, in contrast to the case of $Ra = 10^6$ where the flow is turbulent. In general, the present flow is becoming turbulent at lower Rayleigh numbers because of the low Prandtl number of the liquid metal. It must be noted that only one flow pattern exists for low Rayleigh numbers, while the increase of the Rayleigh number favors a flow separation, forming a secondary flow pattern close to the bottom corner of the cylinder.

Interesting results are obtained in the presence of the magnetic field. For the laminar cases, the flow may or may not be axisymmetric, depending on the magnetic field direction because of the interaction of the Hartmann and side layers. More specifically, axisymmetry is not retained in the case where an horizontal magnetic field is applied, because the magnetic field favors the formation of jets close to the part of the cylindrical wall which is parallel to the magnetic field. The above phenomenon is not observed when the magnetic field is in the axial direction because uniform Hartmann layers are formed in the upper and bottom surfaces and also, azimuthally symmetric side layers are formed near the vertical wall of the cylinder.

As a result of the magnetic damping, the flow in the container is becoming more uniform. The secondary flow pattern that may be formed near the bottom wall always vanishes with increasing Hartmann number, even for the most convective cases. Moreover, when the flow for high Rayleigh numbers is in the turbulent regime, the damping effect of the magnetic field reduces the velocity fluctuations, and for high enough magnetic fields, the flow is laminarized.

The magnetic field has also a significant effect on the heat transfer mechanism. In all cases, the increase of Hartmann number results in a damping of the fluid motion and thus heat conduction progressively dominates over convection heat transfer. For the case of a horizontal magnetic field, the local Nusselt number depends on the azimuthal direction because of the action of the Hartmann and side layers. Finally, the domination of conduction heat transfer is more prominent in the case of an axial magnetic field because of the formation of the Hartmann layer near the upper surface.

Acknowledgements

This work was performed during a mobility stay of the leading author (S.C.K.) in ULB under the cooperation of the Belgian State and Hellenic Republic Associations of EURATOM. I.E.S. was supported by an intra-European EURATOM fellowship (Contract No. 016818). The content of this paper is the sole responsibility of its authors and it does not necessarily represent the views of the Commission or its services.

References

[1] P.A. Davidson, Magnetohydrodynamics in materials processing, Annu. Rev. Fluid Mech. 31 (1999) 273–300.
[2] R. Touihri, H. Ben Hadid, D. Henry, On the onset of convective instabilities in cylindrical cavities heated from below. II. Effect of a magnetic field, Phys. Fluids 11 (8) (1998) 2089–2099.
[3] P.A. Davidson, An Introduction to Magnetohydrodynamics, Cambridge University Press, Cambridge, 2001.
[4] G.M. Oreper, J. Szekely, The effect of a magnetic field on transport phenomena in a Bridgman–Stockbarger crystal growth, J. Crystal Growth 67 (3) (1984) 405–419.
[5] D.H. Kim, P.M. Adornato, R.A. Brown, Effect of vertical magnetic field on convection and segregation in vertical Bringman crystal growth, J. Crystal Growth 89 (2–3) (1988) 339–356.
[6] S. Chandrasekhar, Hydrodynamic and Hydromagnetic Stability, Clarendon, Oxford, 1961.
[7] C. Karcher, Y. Kolesnikov, O. Andreev, A. Thess, Natural convection in a liquid metal heated from above and influenced by a magnetic field, Eur. J. Mech. B/Fluids 21 (16) (2002) 75–90.
[8] J. Baumgartl, G. Mueller, Calculation of the effects of magnetic field damping on fluid flow, Comparison of magnetohydrodynamic models of different complexity, ESA, Proceedings of the Eighth European Symposium on Materials and Fluid Sciences in Microgravity (1992) 161–164.
[9] A.I. Fedoseyev, E.J. Kansa, C. Marin, A.G. Ostrogorsky, Magnetic field suppression of semiconductor melt flow in crystal growth: comparison of three methods for numerical modelling, Jpn. CFD J. 9 (3) (2001) 325–333.
[10] K. Zniper, A. Oubarta, J. Lahjomri, Analytical solution to the problem of heat transfer in an MHD flow inside a channel with prescribed sinusoidal wall heat flux, Energy Convers. Manage. 46 (7–8) (2005) 1147–1163.
[11] I.E. Sarris, I. Lekakis, N.S. Vlachos, Natural convection in a 2D enclosure with sinusoidal upper wall temperature, Numer. Heat Transfer Part A 42 (18) (2002) 513–530.
[12] A.J. Pearlstein, B.P. Dempsey, Low Peclet number heat transfer in a laminar tube flow subjected to axially varying wall heat flux, ASME J. Heat Transfer 110 (3) (2001) 796–798.
[13] A. Barletta, E. Zanchini, Laminar forced convection with sinusoidal wall heat flux distribution: axially periodic regime, Heat Mass Transfer 31 (1–2) (1995) 41–48.
[14] A. Dalal, M.K. Das, Numerical study of laminar natural convection in a complicated cavity heated from top with sinusoidal temperature and cooled from other sides, Comput. Fluids 36 (4) (2007) 680–700.
[15] E. Bilgen, R. Ben Yedder, Natural convection in enclosure with heating and cooling by sinusoidal temperature profiles on one side, Int. J. Heat Mass Transfer 50 (1–2) (2007) 139–150.
[16] I.E. Sarris, S.C. Kakarantzas, A.P. Grecos, N.S. Vlachos, MHD natural convection in a laterally and volumetrically heated square cavity, Int. J. Heat Mass Transfer 48 (16) (2005) 3443–3453.
[17] I.E. Sarris, G.K. Zikos, A.P. Grecos, N.S. Vlachos, On the limits of validity of the low magnetic Reynolds number approximation in MHD natural convection heat transfer, Numer. Heat Transfer Part B 50 (24) (2006) 157–180.
[18] R. Verzicco, P. Orlandi, A finite-difference scheme for three-dimensional incompressible flow in cylindrical coordinates, J. Comput. Phys. 123 (2) (1996) 402–414.
[19] J. Kim, P. Moin, Application of a fractional-step method to incompressible Navier–Stokes equations, J. Comput. Phys. 59 (1985) 308–323.
[20] I.E. Sarris, C.D. Dritselis, A.P. Grecos, N.S. Vlachos, Direct numerical simulation of MHD natural convection cooling in a vertical cylindrical container, in: Proceedings of the First National Conference of Mechanical Electrical Engineers, Athens, Greece, 2005, pp. 42.
[21] S.C. Kakarantzas, A.P. Grecos, N.S. Vlachos, I.E. Sarris, B. Knaepen, D. Carati, Direct numerical simulation of a heat removal configuration for fusion blankets, Energy Convers. Manage. 48 (11) (2007) 2775–2783.
[22] P. Orlandi, Fluid Flow Phenomena: A Numerical Toolkit, Kluwer Academic Press, 2001.
[23] G. Grötzbach, Spatial resolution requirements for direct numerical simulation of the Rayleigh–Bernard convection, J. Comput. Phys. 49 (2) (1983) 241–264.
[24] J.M. Aurnou, P.L. Olson, Experiments on Rayleigh–Bernard convection, magnetoconvection and rotating magnetoconvection in liquid Gallium, J. Fluid Mech. 430 (2001) 283–307.